

Color Correction Meets Cross-Spectral Refinement: A Distribution-Aware Diffusion for Underwater Image Restoration

Laibin Chang, Yunke Wang, Bo Du, *Senior Member, IEEE*, Chang Xu, *Senior Member, IEEE*

Abstract—Underwater imaging often suffers from significant visual degradation, which limits its suitability for subsequent applications. While recent underwater image enhancement (UIE) methods rely on the current advances in deep neural network architecture designs, there is still considerable room for improvement in terms of cross-scene robustness and computational efficiency. Diffusion models have shown great success in image generation, prompting us to consider their application to UIE tasks. However, directly applying them to UIE tasks will pose two challenges, *i.e.*, high computational budget and color unbalanced perturbations. To tackle these issues, we propose *DiffColor*, a distribution-aware diffusion and cross-spectral refinement model for efficient UIE. Instead of diffusing in the raw pixel space, we transfer the image into the wavelet domain to obtain such low-frequency and high-frequency spectra, it inherently reduces the image spatial dimensions by half after each transformation. Unlike single-noise image restoration tasks, underwater imaging exhibits unbalanced channel distributions due to the selective absorption of light by water. To address this, we design the Global Color Correction (GCC) module to handle the diverse color shifts, thereby avoiding potential global degradation disturbances during the denoising process. For the sacrificed image details caused by underwater scattering, we further present the Cross-Spectral Detail Refinement (CSDR) to enhance the high-frequency details, which are integrated with the low-frequency signal as input conditions for guiding the diffusion. This way not only ensures the high-fidelity of sampled content but also compensates for the sacrificed details. Comprehensive experiments demonstrate the superior performance of *DiffColor* over state-of-the-art methods in both quantitative and qualitative evaluations.

Index Terms—Underwater Image Restoration; Distribution-aware Diffusion; Global Color Correction.

I. INTRODUCTION

UNDERWATER clear imaging plays an irreplaceable role in coral reef segmentation [1], marine object detection [2], [3], and autonomous underwater vehicles [4], [5]. However, raw images captured directly from underwater cameras often suffer from various types of degradation, including color deviation, low contrast, and blurred details, caused by the selective absorption and strong scattering of light in water

Laibin Chang and Bo Du are with the School of Computer Science, Institute of Artificial Intelligence, National Engineering Research Center for Multimedia Software, and Hubei Key Laboratory of Multimedia and Network Communication Engineering, Wuhan University, China. (E-mail: changlb666@whu.edu.cn; dubo@whu.edu.cn). (*Corresponding author: Bo Du, Chang Xu.*)

Yunke Wang and Chang Xu are with the School of Computer Science, The University of Sydney, Australia. (E-mail: yunke.wang@sydney.edu.au; c.xu@sydney.edu.au)

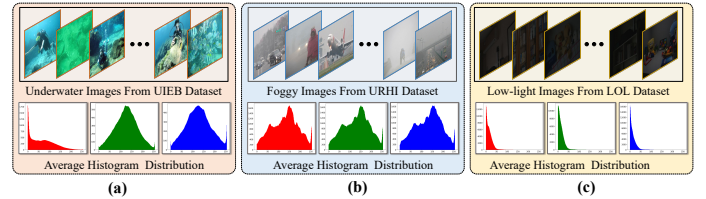


Fig. 1. Average histogram distribution analysis of R-G-B three channels on underwater images, foggy images, and low-light images. (a) the top shows some examples from the underwater benchmark dataset UIEB [17], while the bottom is the average histogram distribution of all images in the UIEB dataset. (b) displays examples and average histogram distribution related to the foggy dataset URHI [18], while (c) illustrates examples and histogram distribution of the low-light dataset LOL [19]. Compared with foggy and low-light scenes, there are significant disparities in the average channel distribution of underwater scenes.

[6]–[10]. Degraded images with these imperfections are not only visually unappealing, but may also impede auxiliary operations for underwater exploration tasks that rely on vision to perceive the surrounding environment. As shown in Fig. 1, compared with single-noise image restoration tasks (low-light enhancement [11]–[14] and defogging [15], [16]), underwater image enhancement (UIE) necessitates removing various noise interferences and equalizing the information distribution across three color channels.

Recently, numerous UIE methods derived from different inspirations have been proposed, ranging from physics-based [20]–[25] to deep learning-based [26]–[35]. These physics-based methods estimate the desired enhancement result from a single degraded image based on underwater imaging priors or pixel-value modification techniques. Despite their success, the effectiveness of these methods depends heavily on the accuracy of hand-crafted priors to improve the visibility of underwater images. However, these priors with invariant parameters are not sufficient to enhance the severely degraded images when confronted with variable underwater environments [29], [36]. Instead of designing hand-crafted priors to improve the visibility of underwater images, deep learning-based solutions can provide relatively satisfactory enhancement results due to their superior data-driven capabilities [34], [37], [38]. However, there are several non-negligible problems with existing deep learning-based methods: 1) The GAN-based UIE methods with adversarial loss occasionally introduce artifacts not present in the clean reference image, leading to noticeable distortion. 2) These methods usually learn non-linear restoration mappings in the raw pixel space of underwater images, with limited exploration and utilization

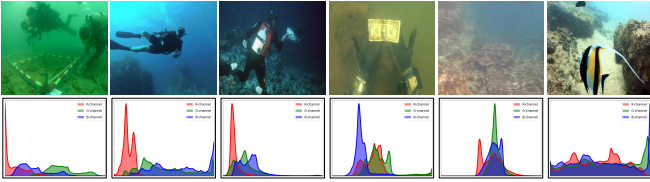


Fig. 2. Underwater images with different degradation types have various information distributions of R-G-B three-color channels.

of spatial properties in the frequency domain of the image, resulting in an ineffective generation of high-quality images. 3) Most methods overlook the distribution disparities across the R-G-B channels in underwater images (as described in Fig. 2) when designing their model architecture.

Diffusion models (DMs) have recently garnered increasing attention due to their impressive performance in image restoration, especially in terms of noise robustness. However, when directly applying DMs to underwater image restoration tasks, they usually require long-time inference to achieve a high-quality mapping from random Gaussian noise to the target image, especially for large-size underwater images. Recently, inspired by the Denoising Diffusion Implicit Models (DDIM) [39] to reduce sampling steps, some DM-based methods [40], [41] have incorporated the skip-sampling strategy to reduce the iterative steps in the denoising process of underwater images. Unfortunately, this manner not only irreversibly sacrifices the high-fidelity of its inherent property to a certain extent, but also fails to exploit spectral information for image restoration. There is a wavelet-based diffusion solution in [42] that demonstrates the effectiveness of decreasing inference time by halving the underwater image resolution after each transformation. However, the proposed model employs a two-stage scheme that establishes two separate diffusion models to restore low-frequency and high-frequency components, which inadvertently increases both the model’s parameter count and computational overhead. In summary, while previous conditional DMs suffice for single-noise restoration tasks in regular images, it should be noted that underwater environments necessitate heightened attention in restoring the global degradation disturbances induced by light attenuation during the reverse denoising process, especially for the color distribution correction and sacrificed detail refinement.

Motivated by the aforementioned analysis, we propose an underwater color corrector (DiffColor) that incorporates distribution-aware diffusion and cross-spectral refinement for efficient underwater image restoration. As depicted in Fig. 3, we initially employ the discrete wavelet transform to transform the degraded image into the wavelet domain, yielding one low-frequency component that characterizes the principal content of the image, along with three high-frequency spectra carrying local details. Instead of operating in the raw image domain with a skip sampling strategy, diffusing on the low-frequency component can reduce the inference time by halving the spatial dimensions after each transformation. This manner also effectively avoids error information accumulation that may occur with non-uniform sampling. In response to the various color shifts caused by the selective absorption of light in water, we design the global color correction (GCC)

module to balance the information distribution across R-G-B three channels in the low-frequency component, thereby preventing the global degradation disturbances that commonly arise during the denoising process. For the sacrificed image details caused by underwater medium scattering, we further propose the cross-spectral detail refinement (CSDR) module to enhance the high-frequency details, which are integrated with the low-frequency signal as input conditions. This way not only maximizes the generative capability of the diffusion model but also compensates for the details sacrificed due to underwater scattering.

Our key contributions are summarized as follows:

- We propose distribution-aware DiffColor to modulate the denoising and avoid global degradation, which is committed to addressing the unbalanced channel distribution caused by underwater light absorption.
- We design the CSDR module to refine image details by exploiting the cross-directional complementarity between different high-frequency spectra and treating them as conditional signals to guide the diffusion.
- Comprehensive experiments demonstrate that DiffColor outperforms existing state-of-the-art UIE solutions in both qualitative and quantitative evaluations.

II. RELATED WORK

A. Underwater Image Enhancement

Underwater image enhancement has garnered widespread attention and can be broadly categorized into physics-based and deep learning-based methods. Early physics-based methods [43]–[45] focused on designing hand-crafted priors to estimate unknown quantities in underwater imaging models, including background light and transmission parameters. Given the similarities between underwater degradation and foggy scenes, several revised DCP-based (Dark Channel Prior) methods have been proposed for underwater image restoration, such as UDCP [46], GDCP [47], and GUDCP [48]. However, there are many disturbing factors affecting underwater imaging, and it is difficult to accurately estimate these environmental parameters. The remaining methods improved the visual perception by directly manipulating image pixel values with well-designed techniques, regardless of the underwater degradation mechanism, including fusion-based [22], [23], [49], [50], Retinex-based [51]–[53], and histogram equalization-based [54]–[56], *etc.* Despite their success, these methods tend to adopt invariant empirical parameters whose poor generalisability cannot cope with complex and changeable underwater scenes.

Deep learning-based methods concentrated on enhancing degraded images by autonomously learning non-linear restoration mappings from paired underwater image datasets. Specifically, many generative adversarial networks (GANs)-based methods have been proposed for underwater image enhancement tasks, such as UGAN [57], WaterGAN [58], FUnIEGAN [59], UWGAN [60], and TwinGAN [61]. However, GAN-based restoration methods with adversarial losses often introduce artifacts that are not present in the pre-processed images during unstable training, and may even fail due to

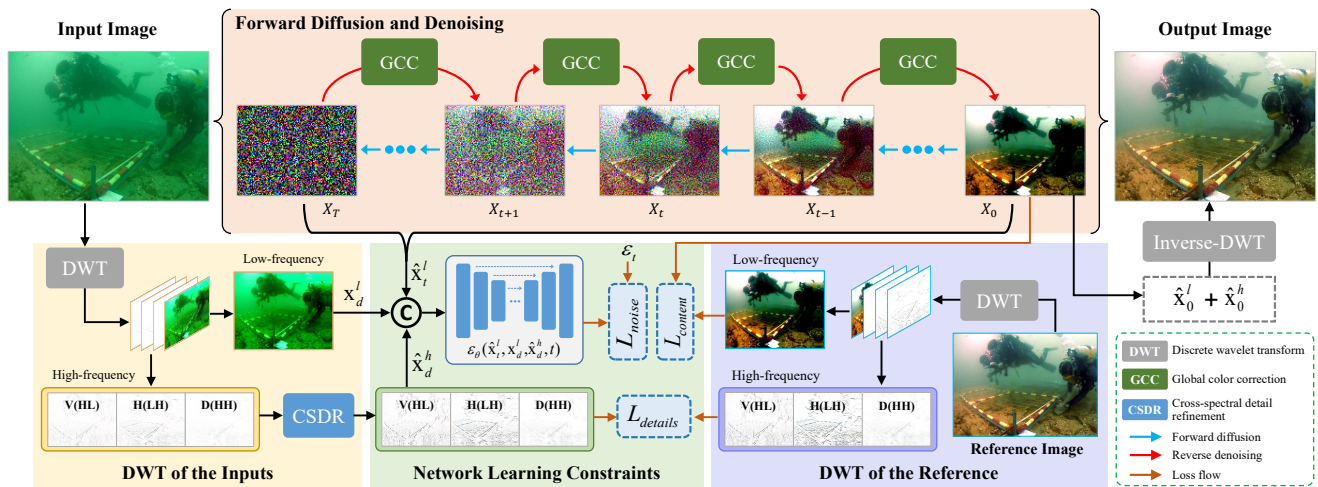


Fig. 3. Overview of the proposed DiffColor. Instead of the raw pixel space, the degraded and reference images are converted into the wavelet domain, yielding one low-frequency component that characterizes the principal content of the image and three high-frequency spectra that represent the image details. For the various color shifts caused by underwater selective absorption, the global color correction (GCC) module is employed to modulate the color information distribution of low-frequency component \hat{x}_d^l during the denoising. For the sacrificed image details caused by underwater medium scattering, the cross-spectral detail refinement (CSDR) module is adopted to enhance the high-frequency details \hat{x}_d^h , which are then integrated with the low-frequency component \hat{x}_d^l as input conditions for the noise estimation network. Finally, the enhanced image is obtained by inverting the generated low-frequency component and three refined high-frequency spectra.

mode collapse. Furthermore, Wang *et al.* [62], [63] proposed the reinforcement learning methods based on Markov decision process (MDP) for underwater image enhancement. Inspired by the revised underwater imaging models, several deep learning methods [64]–[66] have been proposed for reconstructing clear underwater images by estimating the ambient-light and direct-transmission parameters, which are superior to the prior estimation based on a single image. Faced with the noticeable gap between the degradation distributions of real-world underwater images, some end-to-end domain adversarial learning networks have been proposed to promote their adaptive enhancement capabilities, such as TUDA [67], Two-SDA [26], UICoE-Net [30], *etc.* Although these methods attain domain adaption to some extent, most of them have low execution efficiency due to the two-stage model, leaving much room for improvement to meet the underwater real-time processing requirements.

B. Diffusion Model-based Image Restoration

Conditional diffusion-based models have yielded excellent performance with their powerful generative capabilities and have been applied in a variety of image restoration tasks, including low-light enhancement [68], [69], super-resolution [70], inpainting [71], deblurring [72], *etc.* In the field of underwater image restoration, Lu *et al.* [73] proposed an underwater image enhancement method called UW-DDPM, which utilizes two U-Net networks to perform denoising and distribution transforms. Although UW-DDPM is superior to the GAN-based UIE methods, the multiple forward and reverse passes throughout the whole network usually require a substantial amount of computational resources. Inspired by the idea of reducing sampling in [39], Tang *et al.* [40] introduced a lightweight transformer-based denoising diffusion network for underwater image enhancement and adopted a

skip sampling strategy to reduce backward iteration steps. Then, Lu *et al.* [41] accelerated the inference process of UIE by modifying the initial sampling distribution and reducing the number of iterations in the denoising phase. However, these diffusion-based underwater image enhancement methods only operate in the raw image domain, and have limited exploration and utilization of the spatial characteristics in the image frequency domain. Recently, Zhao *et al.* [42] proposed a wavelet-based diffusion model named WF-Diff to enhance underwater images, which includes the wavelet-based Fourier information interaction network and frequency residual diffusion adjustment network. However, WF-Diff is a two-stage scheme that initially utilizes frequency information exchange to obtain coarse results, and then designs two separate diffusion models to respectively restore low-frequency and high-frequency components, inevitably exacerbating the model's parameters and computational burden.

III. METHODOLOGY

A. Motivation Stems From Two Challenges

Heavy Computational Burdens and Frequency Domain Exploitation. Reducing the resolution of large-scale images with a down-sampling operation can significantly decrease the computational resources required by the diffusion model. However, this down-sampling way will irreversibly lead to the loss of image information during the inverse process. The Discrete Wavelet Transform (DWT) can effectively halve the resolution of the input image after each transformation, converting it into a low-frequency component and three high-frequency details without sacrificing information. In addition, learning non-linear restoration mappings in the raw pixel space of underwater images is limited, while exploring and utilizing spatial characteristics in the frequency domain can aid in generating high-quality images. Hence, we utilize the DWT

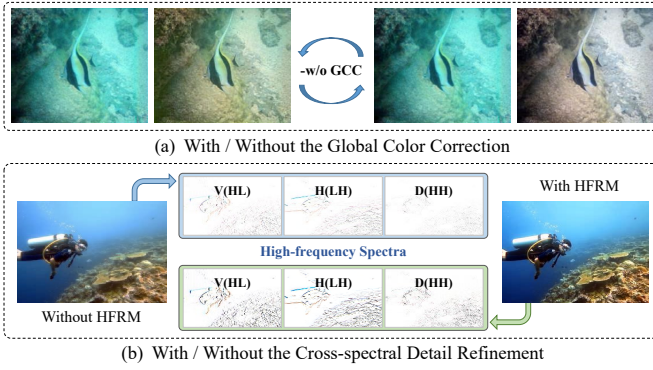


Fig. 4. Ablation comparison regarding the necessity of the GCC and CSDR modules. (a) The GCC module corrects the global degradation caused by underwater selective absorption. (b) The CSDR module refines the image details sacrificed due to underwater medium scattering.

to transform the degraded image into the wavelet domain, yielding a halved low-frequency component and three complementary high-frequency spectra.

Global Degradation Caused by Underwater Absorption and Scattering. In contrast to natural images captured from landscapes, underwater image degradation is mainly interfered with selective absorption and medium scattering in water. Specifically, underwater selective absorption leads to color deviation in degraded images, while medium scattering causes their details to appear blurred. Taking into account both color correction and detail refinement in a limited number of sampling steps is a significant challenge for diffusion models, especially for dealing with underwater images with more severe degradation. As shown in Fig. 4, we not only need to correct for biased colors with the Global Color Correction (GCC) module, but also enrich the sacrificed details with the Cross-Spectral Detail Refinement (CSDR) in the whole restoration process.

B. Frequency-guided Conditional Diffusion

Considering the generative capability of the diffusion model and the dimensionality reduction advantages of the discrete wavelet transform, we incorporate these two designs and propose the underwater distribution-aware diffusion model (DiffColor) to enhance underwater images. As depicted in Fig. 3, we perform the diffusion operations in the wavelet domain instead of the image space by transforming the degraded image into low-frequency and high-frequency components. In addition, we adopt the GCC module to correct the unbalanced color distribution caused by selective absorption, and introduce the CSDR module to refine the local texture details sacrificed due to medium scattering.

Given a degraded underwater image $X_d \in \mathbb{R}^{H \times W \times 3}$ and its corresponding reference $X_0 \in \mathbb{R}^{H \times W \times 3}$, we utilize the two-dimensional DWT with Haar wavelet to transform them into wavelet spectra with four sub-bands, respectively. The Haar wavelet consists of a low-pass filter L and a high-pass filter H , and their expressions are as follows:

$$L = \frac{1}{\sqrt{2}} \begin{bmatrix} 1 & 1 \end{bmatrix}, \quad H = \frac{1}{\sqrt{2}} \begin{bmatrix} -1 & 1 \end{bmatrix}. \quad (1)$$

The two filters L and H are used for constructing four kernels with stride 2, including LL^T , HL^T , LH^T , and HH^T . These kernel functions transform the input images X_d and X_0 into a low-frequency component and three high-frequency spectra, which are expressed as follows:

$$\{x_d^l, x_d^h, x_0^l, x_0^h\} = DWT(X_d, X_0), \quad (2)$$

where $\{x_d^l, x_0^l\} \in \mathbb{R}^{\frac{H}{2} \times \frac{W}{2} \times 3}$ represent the low-frequency components, and $\{x_d^h, x_0^h\} \in \mathbb{R}^{\frac{H}{2} \times \frac{W}{2} \times 9}$ represent the high-frequency spectra, encompassing three directions of the vertical $\{V_d, V_0\} \in \mathbb{R}^{\frac{H}{2} \times \frac{W}{2} \times 3}$, horizontal $\{H_d, H_0\} \in \mathbb{R}^{\frac{H}{2} \times \frac{W}{2} \times 3}$, and diagonal $\{D_d, D_0\} \in \mathbb{R}^{\frac{H}{2} \times \frac{W}{2} \times 3}$, respectively. The low-frequency component x_d^l is involved in the inference process of the diffusion model to restore the global content, while the high-frequency spectral bands x_d^h serve as indispensable conditions to enrich the local details.

During the forward diffusion, we gradually add Gaussian random noise to the low-frequency component x_d^l in T steps, following $q(\hat{x}_t^l | x_0^l) = \mathcal{N}(\hat{x}_t^l; \sqrt{\alpha_t} x_0^l, (1 - \alpha_t) \mathbf{I})$, $t = 1, 2, \dots, T$. Considering that the spatial dimension of the low-frequency component is halved after each transformation, diffusion on this component effectively reduces the computational burden of the noise estimation network. This way also avoids the error-prone information accumulation associated with a multi-scale sampling strategy. Besides, we adopt a lightweight cross-spectral detail refinement (CSDR) to enhance the high-frequency spectral distribution between the degraded image and the clearer version, with the following loss function expressed as follows:

$$\mathcal{L}_{details} = \sum_{k=1}^K \left\| \{\hat{V}_d^k, \hat{H}_d^k, \hat{D}_d^k\} - \{V_0^k, H_0^k, D_0^k\} \right\|^2, \quad (3)$$

where K represents the total number of wavelet transforms and k represent k -th wavelet scale.

Instead of the traditional diffusion model only taking the degraded image X as a condition, we jointly incorporate the sampled results \hat{x}_t^l , the low-frequency component x_d^l , and the enriched high-frequency coefficients \hat{x}_d^h as conditional inputs for the denoising network $\epsilon_\theta(\hat{x}_t^l, x_d^l, \hat{x}_d^h, t)$, ensuring the high-fidelity of the restored content even if starting from a randomly sampled noise. This way not only maximizes the generative capability of the diffusion model but also compensates for the details sacrificed due to underwater scattering. Based on this, the objective loss function is defined as:

$$\mathcal{L}_{noise} = \mathbb{E}_{x_0, \epsilon_t \sim \mathcal{N}(0, \mathbf{I})} \|\epsilon_t - \epsilon_\theta(\hat{x}_t^l, x_d^l, \hat{x}_d^h, t)\|^2, \quad (4)$$

where $t = 1, 2, \dots, T$. ϵ_t and ϵ_θ represent the noise added at time t and the predicted noise, respectively.

In addition, we define a content loss function $\mathcal{L}_{content}$ to ensure the content consistency between the restored low-frequency component \hat{x}_d^l and target sample x_0^l , accomplished through the minimization of their L_1 distance and structural similarity. This content-based constraint function $\mathcal{L}_{content}$ is customized as follows:

$$\mathcal{L}_{content} = \|\hat{x}_d^l - x_0^l\|_1 + (1 - SSIM(\hat{x}_d^l, x_0^l)). \quad (5)$$

Algorithm 1: The Training of DiffColor

Input: Degraded and clear images, denoted as \bar{X}_d and X_0 ; Noise schedule β_t ; Noise estimation network θ ; Diffusion steps T and sampling steps S .

Repeat

- 1: # *Discrete wavelet transform*
- 2: $\{x_d^l, x_d^h, x_0^l, x_0^h\} = DWT(X_d, X_0)$
- 3: # *Refine high-frequency components*
- 4: $\hat{x}_d^h = CSDR(x_d^h)$
- 5: # *Forward diffusion process*
- 6: Sample $t \sim \text{Uniform}\{1, 2, \dots, T\}$
- 7: Sample $\epsilon_t \sim \mathcal{N}(0, \mathbf{I})$
- 8: $\hat{x}_t^l = \sqrt{1 - \beta_t}x_{t-1}^l + \beta_t\epsilon_t$
- 9: Perform a single gradient descent step on $\nabla_{\theta} \|\epsilon_t - \epsilon_{\theta}(\hat{x}_t^l, x_d^l, \hat{x}_d^h, t)\|^2$
- 10: # *Reverse denoising process*
- 11: Sample $x_T \sim \mathcal{N}(0, \mathbf{I})$
- 12: Sample $\alpha_t = 1 - \beta_t$ and $\bar{\alpha}_t = \prod_{i=1}^t \alpha_i$
- 13: **for** $i = S$ to 1 **do**
- 14: $t = (i - 1) \cdot T/S + 1$
- 15: $t - 1 = (i - 2) \cdot T/S + 1$ if $i > 1$, else 0
- 16: $\hat{x}_{t-1}^l = \frac{1}{\sqrt{\alpha_t}}(\hat{x}_t^l - \frac{(1-\alpha_t)}{\sqrt{1-\bar{\alpha}_t}}\epsilon_{\theta}(\hat{x}_t^l, x_d^l, \hat{x}_d^h, t)) + \frac{(1-\alpha_t)(1-\bar{\alpha}_{t-1})}{1-\bar{\alpha}_t}$
- 17: # *Global color correction*
- 18: $\hat{x}_{t-1}^l = GCC(\hat{x}_{t-1}^l)$
- 19: **end for**
- 20: Perform a single gradient descent step on
- 21: $\nabla_{\theta} \|\hat{x}_d^l - x_0^l\|^2$ and $\nabla_{\theta} \|\hat{x}_d^h - x_0^h\|^2$

Until converged

Algorithm 2: The Inference of DiffColor

Input: Degraded image X_d ; Noise schedule β_t ; Noise estimation network θ ; Diffusion steps T and sampling steps S .

- 1: # *Discrete wavelet transform*
 - 2: $\{x_d^l, x_d^h\} = DWT(X_d)$
 - 3: # *Refine high-frequency components*
 - 4: $\hat{x}_d^h = CSDR(x_d^h)$
 - 5: # *Reverse denoising process*
 - 6: Sample $x_T \sim \mathcal{N}(0, \mathbf{I})$
 - 7: Sample $\alpha_t = 1 - \beta_t$ and $\bar{\alpha}_t = \prod_{i=1}^t \alpha_i$
 - 8: **for** $i = S$ to 1 **do**
 - 9: $t = (i - 1) \cdot T/S + 1$
 - 10: $t - 1 = (i - 2) \cdot T/S + 1$ if $i > 1$, else 0
 - 11: $\hat{x}_{t-1}^l = \frac{1}{\sqrt{\alpha_t}}(\hat{x}_t^l - \frac{(1-\alpha_t)}{\sqrt{1-\bar{\alpha}_t}}\epsilon_{\theta}(\hat{x}_t^l, x_d^l, \hat{x}_d^h, t)) + \frac{(1-\alpha_t)(1-\bar{\alpha}_{t-1})}{1-\bar{\alpha}_t}$
 - 12: # *Global color correction*
 - 13: $\hat{x}_{t-1}^l = GCC(\hat{x}_{t-1}^l)$
 - 14: **end for**
 - 15: # *Inverse discrete wavelet transform*
 - 16: $I_{out} = IDWT(\hat{x}_0^l, \hat{x}_d^h)$
 - 17: **Return** I_{out}
-

refinement term $\mathcal{L}_{details}$, and the content preservation term $\mathcal{L}_{content}$, the total objective function \mathcal{L}_{total} is defined by combining them as follows:

$$\mathcal{L}_{Total} = \mathcal{L}_{noise} + \lambda \mathcal{L}_{details} + \mathcal{L}_{content}, \quad (6)$$

where $\lambda = 0.1$ is weighted to coordinate the significance of details refinement with the other two terms in the experiment.

By transforming the input image from the image domain to the wavelet domain, its spatial dimension is reduced, thereby improving the restoration efficiency while leveraging the powerful generation capability of the diffusion model. The enriched three high-frequency spectra $\hat{x}_0^h \in \{\hat{V}_0^k, \hat{H}_0^k, \hat{D}_0^k\}$ at scale k -th and their corresponding restored low-frequency component \hat{x}_0^l are transformed to the final enhanced result by employing the Inverse Discrete Wavelet Transform (IDWT), expressed as follows:

$$I_{out} = IDWT(\hat{x}_0^l, \{\hat{V}_0^k, \hat{H}_0^k, \hat{D}_0^k\}), \quad (7)$$

where I_{out} represents the final restored image. Algorithm 1 and Algorithms 2 present the specific training and inference processes, respectively.

C. Low-frequency Color Correction via Conditional Sequential Modulation

Underwater degraded images usually exhibit a wide variety of degradation appearances due to the unbalanced distribution of color channels resulting from the light selective absorption, as shown in Fig. 2. However, these various intra-domain color shifts cannot be adequately corrected with diffusion models alone, which has been experimentally demonstrated in [74]. Guided by the principle [21] that natural images typically exhibit similar channel distributions, we propose an adaptive color correction method to modulate the three-channel information of the sampled results during the reverse denoising.

As depicted in Fig. 5 (a), the global color correction (GCC) module mainly consists of a conditional prediction network and a feature-modulated baseline network. The baseline network employs a fully convolutional structure with a size of 1×1 to ensure that each pixel in the input image is manipulated independently, while the conditional predictor network uses dilated convolution to ensure that the global prior can be propagated to the base network in the manner of feature modulation. The condition network resembles an encoded predictor, comprising three stride convolution blocks for generating a 32-dimensional 1×1 vector from the input image, *i.e.*, conditional predictor. Specifically, the network comprises three Strided Convolutional layers, each with a channel size of 32. The kernel size of the first Strided Convolutional layer is set to 7×7 to increase the receptive field, while the last two layers are 3×3 . Each strided convolutional layer sets the stride to 2 and downsamples the feature map to half. At the end of the condition network, the Global Average Pooling (GAP) layer is used to obtain a 1×1 32-dimensional vector. Finally, the predictor generates conditional parameters based on the degradation features of underwater images, which are

Based on the noise estimation term \mathcal{L}_{noise} , the details

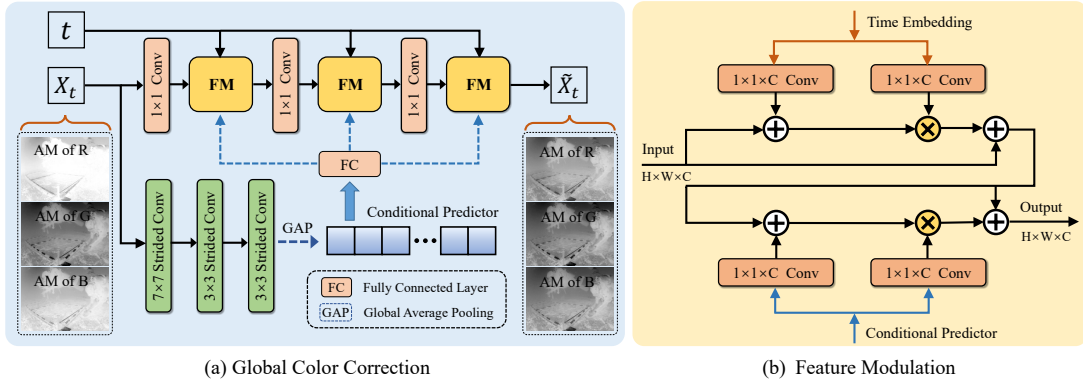


Fig. 5. The detailed architecture of the Global Color Correction (GCC) module and Feature Modulation (FM) block. The GCC module consists of a conditional sequence network and a baseline network with feature modulation.

then propagated in a fully connected manner to the baseline network for image correction.

The conditional network estimates a global degradation prior from the input underwater image, which is then propagated to the baseline network to assist in correcting the RGB channel information. Given a feature x with the shape of $H \times W \times C$, the instance-level normalization method [75] is calculated on the feature x by subtracting the mean $\mu(x)$ and then dividing by the standard deviation $\sigma(x)$, which is expressed as follows:

$$F_{out}(x) = \gamma \frac{x - \mu(x)}{\sigma(x)} + \beta, \quad (8)$$

where $\mu(x)$ and $\sigma(x)$ are the mean and standard deviation of the input feature map x , and $\gamma, \beta \in \mathbb{R}^C$ are scalable parameters learned from data distribution.

To facilitate global prior estimation, we revised the normalization manner to achieve the color correction of the generated image X_t only through scaling and shifting operations. The revised feature modulation (FM) only requires γ and β to scale and shift the feature map x without normalizing it. Thus, the normalization operation in Eq. (8) can be modified as $F_{out}(x) = \gamma * x + \beta$. Fig. 5 (b) illustrates the detailed structure of the FM module, which mainly modulates channel features with these affine parameters generated by the conditional prediction network. Since the gradual reduction of noise during inverse inference is crucial prior information, we ensure that the corrected results establish a certain correspondence with the noise level by adding time embedding t , serving as an input to the feature modulation. As illustrated in Fig. 5 (a), the channel attenuation map (AM) of the corrected image \hat{X}_t using the GCC module achieves a balanced distribution, whereas the input sampled result X_t exhibit significant attenuation.

D. High-frequency Details Refinement via Cross-spectral Content Collaboration

Underwater imaging is affected by medium scattering, resulting in blurred image details and even sacrificing many crucial pieces of information. However, many previous methods have focused on correcting the color cast in enhancing underwater images, and tend to neglect the high-frequency refinement that carries more texture information. To remedy

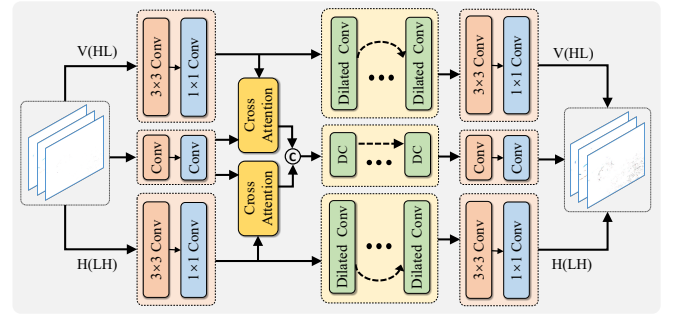


Fig. 6. The detailed architecture of the Cross-spectral Detail Refinement module (CSDR). It includes six groups of 3×3 and 1×1 convolutional layers, three dilated convolutional blocks, and two cross-attention layers that compensate for diagonal information by relying on vertical and horizontal high-frequency components.

their shortcomings, we introduce a Cross-spectral Detail Refinement (CSDR) to enhance the sacrificed image details.

The discrete wavelet transform divides the high-frequency spectrum of an image into vertical, horizontal, and diagonal components, each of which exhibits complementary interdependencies. Benefiting from this property, we design the CSDR module that leverages the vertical and horizontal information to compensate for the sacrificed details in the diagonal. As shown in Fig. 6, the three high-frequency components $\{V_d^k, H_d^k, D_d^k\}$ are sequentially extracted by three 3×3 and 1×1 Convolutional layers, and then two Cross-attention layers [82] are employed to utilize vertical $\{V_d^k\}$ and horizontal $\{H_d^k\}$ information to restore the details in diagonal $\{D_d^k\}$. Specifically, taking the high-frequency components $\{V_d^k\}$ and $\{D_d^k\}$ as examples, we calculate the corresponding query vector $Q_{vd} = query(V_d^k)$, key vector $K_{vd} = key(D_d^k)$, and value vector $V_{vd} = key(D_d^k)$, respectively. Then, the first output feature F_{VD} of the cross attention block are calculated as follows:

$$F_{VD} = Softmax \left(\frac{Q_{vd} K_{vd}^T}{\sqrt{d_x}} V_{vd} \right), \quad (9)$$

where d_x denotes the dimension of the key vector K_{vd} . Similarly, we can calculate the corresponding cross-attention feature result F_{HD} based on the horizontal and diagonal high-frequency components in the same manner.

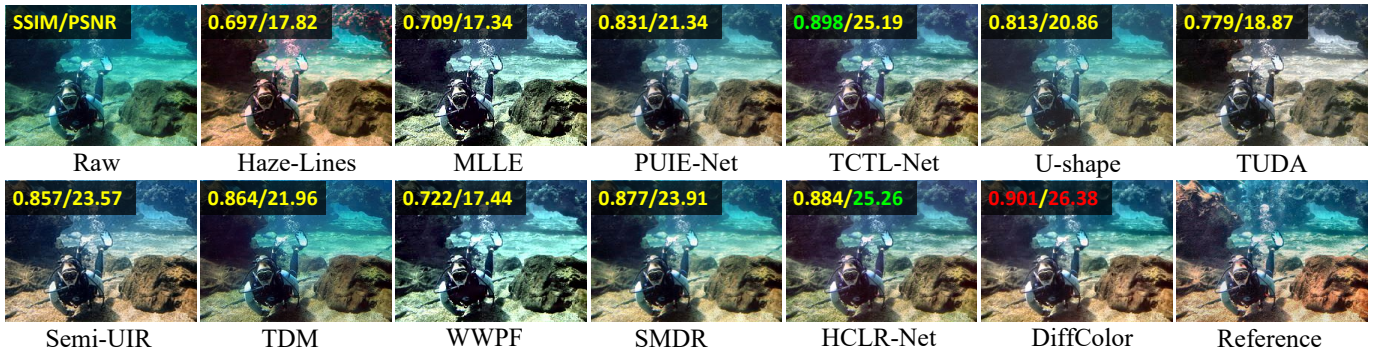


Fig. 7. Qualitative results of testing images from the full-reference underwater benchmark *Test-U100*. From left to right: Input image, Haze-Lines [76], MLLE [20], PUIE-Net [77], TCTL-Net [78], U-shape [79], TUDA [67], Semi-UIR [29], TDM [40], WWPF [80], SMDR [81], HCLR-Net [27], our DiffColor, and the clear reference.

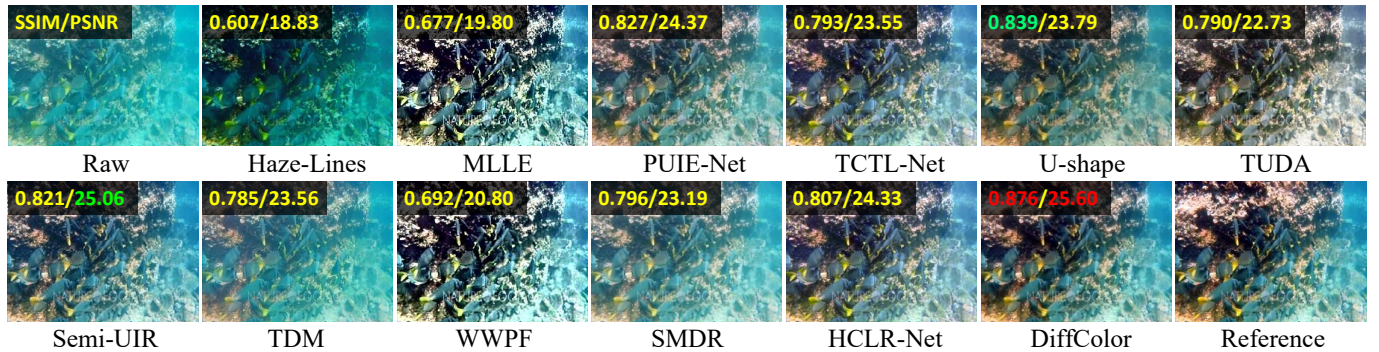


Fig. 8. Qualitative results of testing images from the full-reference underwater benchmark *Test-L500*. From left to right: Input image, Haze-Lines [76], MLLE [20], PUIE-Net [77], TCTL-Net [78], U-shape [79], TUDA [67], Semi-UIR [29], TDM [40], WWPF [80], SMDR [81], HCLR-Net [27], our DiffColor, and the clear reference.

To increase the receptive field of the input, we adopt the Dilated Convolutional blocks with a progressive dilation rate for feature extraction, in which the first and last layers are used to extract local information, and the middle layers improve global information utilization by expanding the receptive field. By setting the dilation rates as $d = \{1, 2, 3, 2, 1\}$, this gradual increase and decrease effectively avoids grid effects. Finally, three refined high-frequency components $\{\hat{V}_d^k, \hat{H}_d^k, \hat{D}_d^k\}$ are obtained by reducing the channel dimensions with three 3×3 and 1×1 Convolutional layers. As a whole, the CSDR module sensibly leverages the complementary advantages of the three high-frequency components $\{V_d^k, H_d^k, D_d^k\}$ to refine the textural details of degraded images.

IV. EXPERIMENT AND ANALYSIS

A. Experimental Settings

Implementation Details. The proposed DiffColor is trained using the Pytorch framework on two NVIDIA GeForce RTX 4090 GPUs for 500 epochs. During the training phase, the batch size and patch size are set to 16 and 256×256 , respectively. The Adam optimizer comes with an initial learning rate of 1×10^{-4} and decreases it by a factor of 0.8 after every fifty epochs. The diffusion time step is set to $T = 200$, while the sampling step is set to $S = 10$ for efficient restoration. The number of wavelet transforms is set to 2, and the resolution of the low-frequency component is reduced to 1/4 of the original input image.

Underwater Image Datasets. Our experiments include paired image benchmarks (UIEB [17], EUVP [59], and LSUI [79]), consisting of real-world underwater images with ground truth references. The benchmarks of RUIE [83], SQUID [76], and UDD [84] lack paired images and instead comprise degraded single underwater images. Specifically, following [40], [67], we utilize 790 images from the UIEB dataset and 3779 images from the LSUI dataset for training. The remaining 100 and 500 underwater images in UIEB and LSUI are designated as Test-U100 and Test-L500 for testing, respectively. During testing, images required for the full-reference evaluation primarily originate from EUVP, Test-U100, and Test-L500, while the non-reference evaluation relies on the benchmarks of RUIE, SQUID, and UDD.

Comparison with the SOTA Methods. We compare the proposed DiffColor with eleven state-of-the-art (SOTA) underwater image enhancement methods, including Haze-Lines [76], MLLE [20], PUIE-Net [77], TCTL-Net [78], U-shape [79], TUDA [67], Semi-UIR [29], TDM [40], WWPF [80], SMDR [81], and HCLR-Net [27]. Among these methods, Haze-Lines, MLLE, and WWPF are three physical-based methods, while PUIE-Net, TCTL-Net, U-shape, TUDA, Semi-UIR, TDM, SMDR, and HCLR-Net are seven deep learning-based methods.

Evaluation Metrics. For paired images, we adopt three full-reference metrics to evaluate the enhancement performance of each method, including UIF [85], SSIM, and PSNR. Meanwhile, for these unpaired images, the results are evaluated with

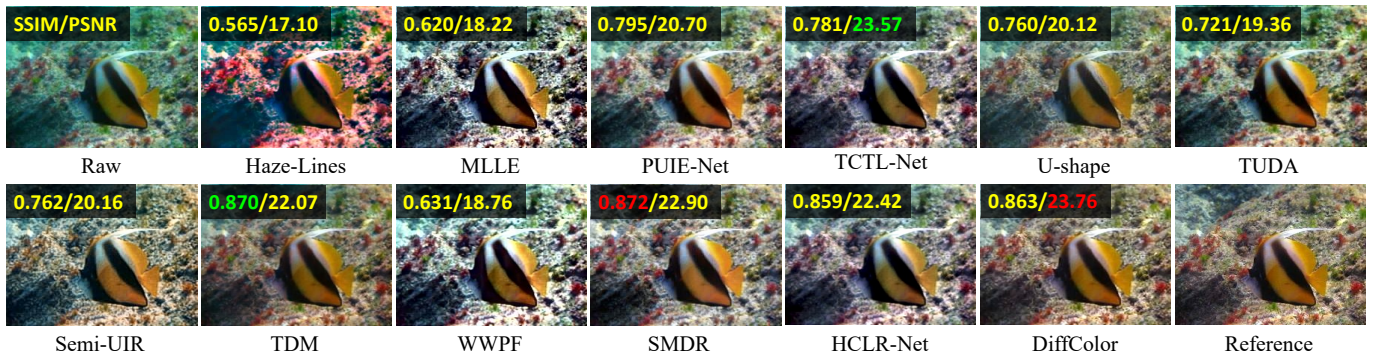


Fig. 9. Qualitative results of testing images from the full-reference underwater benchmark *EUVP* [59]. From left to right: Input image, Haze-Lines [76], MLE [20], PUIE-Net [77], TCTL-Net [78], U-shape [79], TUDA [67], Semi-UIR [29], TDM [40], WWPF [80], SMDR [81], HCLR-Net [27], our DiffColor, and the clear reference.

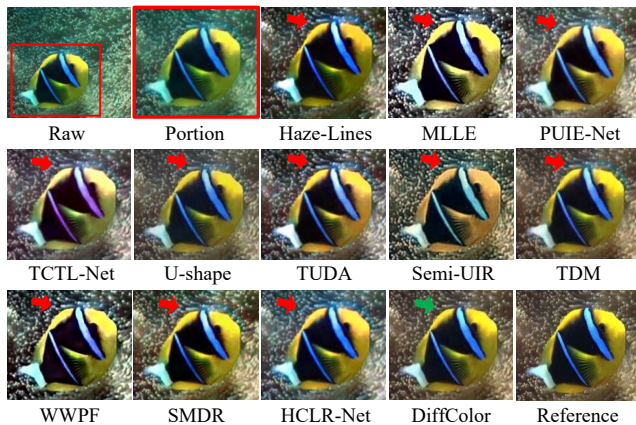


Fig. 10. Qualitative comparison of color and details preservation. DiffColor achieves the most homogeneous visual perception and does not introduce blue-green artifacts around the fish, as observed in other methods (marked with red arrows).

UCIQE [86] and UIQM [87], which are popular non-reference metrics for evaluating underwater images. Specifically, UIF utilizes statistical features in CIELab space to evaluate underwater images in terms of naturalness, clarity, and structural indexes. The UCIQE metric is used to evaluate the quality of color distribution in the Lab color space. The UIQM consists of three attributes called UICM, UISM, and UIConM, which are used to evaluate the color, clarity, and contrast of underwater image perception, respectively. Throughout the experiment, we maintain the parameters suggested in the respective papers for each metric.

B. Qualitative Evaluation with Naturalness

We first compare the proposed DiffColor and ten SOTA methods on three full-reference underwater datasets, including Test-U100, Test-L500, and EUVP. The enhancement results on three underwater datasets are showcased in Fig. 7, Fig. 8, and Fig. 9, respectively. In the visual comparison, even though most methods have achieved satisfactory enhancement results, our method demonstrates the closest perception to the reference in terms of color saturation, content similarity, and global contrast. Considering the subjectivity of individual visual perception, we further employ two commonly used image quality evaluation metrics (SSIM and PSNR) to compare the

enhancement results of each method. As shown in Fig. 7-9, the results show that our method achieves the best scores on all three datasets of Test-U100, Test-L500, and EUVP. Semi-UIR and HCLR-Net achieved the second-best scores on both test-U100 and Test-L500 datasets, while TUDA and TDM achieved relatively satisfactory results on the sample image from the EUVP benchmark. To verify the color fidelity of each method in handling underwater images, we conducted a detailed comparison with respect to color preservation. As shown in Fig. 10, our DiffColor achieves the most homogeneous visual perception and does not introduce blue-green artifacts around the fish as observed in other methods. Overall, our DiffColor surpasses several state-of-the-art underwater image enhancement methods on reference datasets.

C. Quantitative Evaluation with Metrics

The results of quantitative evaluation in Test-U100, Test-L500, and EUVP are presented in Table I. Our proposed DiffColor achieves the best results in terms of UIF, SSIM, and PSNR metrics. The potential reason is the robust generative capability of the designed diffusion model, coupled with the CSDR and GCC modules that focus on image detail richness and color correction. For the SSIM metric, HCLR-Net, U-shape, and TDM methods achieve the second-best results on Test-U100, Test-L500, and EUVP benchmarks, respectively. In addition, Semi-UIR and PUIE-Net methods obtain the second-best scores on Test-U100 and EUVP datasets in terms of PSNR metrics, respectively.

D. Evaluation of Model Efficiency

We analyze the model efficiency of DiffColor compared to other methods on Test-U100, Test-L500, and EUVP benchmarks. The comparative experiment covers four aspects: Parameters, FLOPs, inference time, and FPS, with the results depicted in Fig. 11 and Fig. 12. All experiments regarding efficiency evaluation are conducted on the same device to ensure fairness across methods.

Parameters and FLOPs Evaluation. We conduct comparisons between DiffColor and deep learning-based methods in terms of Parameters and FLOPs. As shown in Fig. 11, we can observe that the FLOPs of DiffColor are the lowest. This is attributed to the introduction of wavelet transform,

TABLE I
 QUANTITATIVE EVALUATION OF FULL-REFERENCE METRICS ON THREE UNDERWATER DATASETS (*Test-U100*, *Test-L500*, AND *EUVP*). THE BEST AND SECOND-BEST RESULTS ARE HIGHLIGHTED WITH **BOLD** AND UNDERLINED, RESPECTIVELY.

Methods	Test-U100			Test-L500			EUVP			Average		
	UIF↑	SSIM↑	PSNR↑	UIF↑	SSIM↑	PSNR↑	UIF↑	SSIM↓	PSNR↓	UIF↑	SSIM↓	PSNR↓
Haze-Lines [76]	0.435	0.616	16.376	0.416	0.551	19.786	0.343	0.563	18.652	0.359	0.563	18.774
MLLE [20]	0.405	0.631	16.660	0.365	0.632	19.202	0.347	0.584	17.268	0.352	0.594	17.593
PUIE-Net [77]	0.486	0.825	21.841	0.454	0.821	24.354	<u>0.417</u>	0.802	22.778	<u>0.426</u>	0.806	23.027
TCTL-Net [78]	0.512	0.906	<u>25.357</u>	0.445	0.788	22.830	0.407	0.736	21.781	0.418	0.751	22.098
U-shape [79]	0.476	0.816	21.826	0.446	0.849	<u>24.631</u>	0.410	0.819	<u>23.392</u>	0.419	0.824	<u>23.558</u>
TUDA [67]	0.491	0.787	18.239	0.441	0.793	21.703	0.407	0.723	20.277	0.416	0.738	20.460
Semi-UIR [29]	0.493	0.852	23.636	0.433	0.815	24.070	0.394	0.796	22.107	0.405	0.801	22.514
TDM [40]	0.454	0.876	21.657	0.463	0.793	24.470	0.408	0.889	23.277	0.420	0.871	23.433
WWPF [80]	0.446	0.711	17.571	0.389	0.680	19.419	0.361	0.642	18.038	0.369	0.651	18.269
SMDR [81]	0.496	0.870	23.575	0.448	<u>0.855</u>	24.219	0.411	<u>0.880</u>	22.647	0.421	<u>0.875</u>	22.963
HCLR-Net [27]	0.491	0.882	25.174	0.449	0.836	23.656	0.413	0.856	22.747	0.422	0.853	22.997
DiffColor	<u>0.498</u>	<u>0.891</u>	26.165	<u>0.461</u>	0.861	25.636	0.433	0.879	23.518	0.440	0.876	23.993

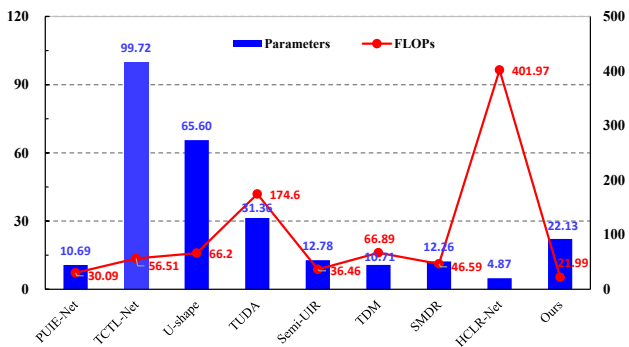


Fig. 11. Efficiency of each deep learning-based method with Parameters (M) and FLOPs (G).

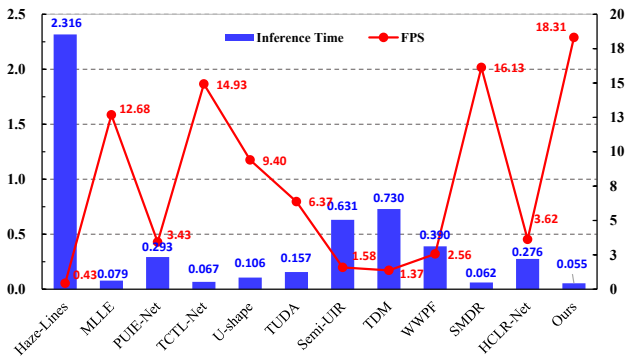


Fig. 12. Efficiency of each method with Inference Time (s) and FPS.

which reduces the image size, thereby significantly reducing the model’s computational overhead. As for the number of parameters, DiffColor is also relatively lightweight compared to TCTL-Net, U-shape, and TUDA methods. Thus, considering both the Params and FLOPs, DiffColor is better suited than other state-of-the-art methods for embedded processors with limited computational power in underwater vehicles.

Inference Time and FPS Evaluation. We further conducted a comparative analysis of the average inference time and Frames Per Second (FPS) of each method. As shown in Fig. 12, the proposed DiffColor outperforms both physics-based and deep learning-based state-of-the-art methods. In terms of inference time per image, our DiffColor accelerates over 13.5% compared to the second fastest SMDR model and surpasses it by 2.19 (18.31 for DiffColor and 16.13 for SMDR)

in the FPS metric. Notably, when applied to real-time processing tasks for underwater videos in real-world applications, the advantages of the proposed method are particularly evident.

TABLE II
 ABLATION STUDIES OF GCC AND CSDR MODULES. “-w/o” MEANS THERE IS NO CORRESPONDING MODULE.

Datasets	-w/o GCC		-w/o CSDR		All	
	SSIM↑	PSNR↑	SSIM↑	PSNR↑	SSIM↑	PSNR↑
Test-U100	0.783	18.908	0.856	22.780	0.891	26.165
Test-L500	0.775	20.936	0.832	21.089	0.861	25.636
EUVP	0.801	17.865	0.861	20.106	0.879	23.518

TABLE III
 ABLATION STUDIES OF THE LOSS FUNCTIONS. “-w/o” MEANS THERE IS NO CORRESPONDING LOSS.

Datasets	-w/o $\mathcal{L}_{details}$		-w/o $\mathcal{L}_{content}$		All	
	SSIM↑	PSNR↑	SSIM↑	PSNR↑	SSIM↑	PSNR↑
Test-U100	0.856	22.786	0.817	20.076	0.891	26.165
Test-L500	0.843	21.341	0.798	19.713	0.861	25.636
EUVP	0.848	21.543	0.809	19.858	0.879	23.518

TABLE IV
 ABLATION STUDIES OF THE CONDITIONAL INPUTS.

Datasets	-w/o HF-Conditions		All	
	SSIM↑	PSNR↑	SSIM↑	PSNR↑
Test-U100	0.829	23.018	0.891	26.165
Test-L500	0.816	22.422	0.861	25.636
EUVP	0.831	22.205	0.879	23.518

E. Ablation Study

To analyze the effectiveness of each component in our DiffColor method, we also conduct an ablation study on Test-U100, Test-L500, and EUVP benchmarks. Fig 13 shows the qualitative results of the ablation contribution for each key component. These results demonstrate that the absence of high-frequency detail refinement leads to the blurring of details in Fig. 13 (c)(f), while without color correction fails to entirely remove the color cast in Fig. 13 (b). In addition, Fig. 13 (d)(e)

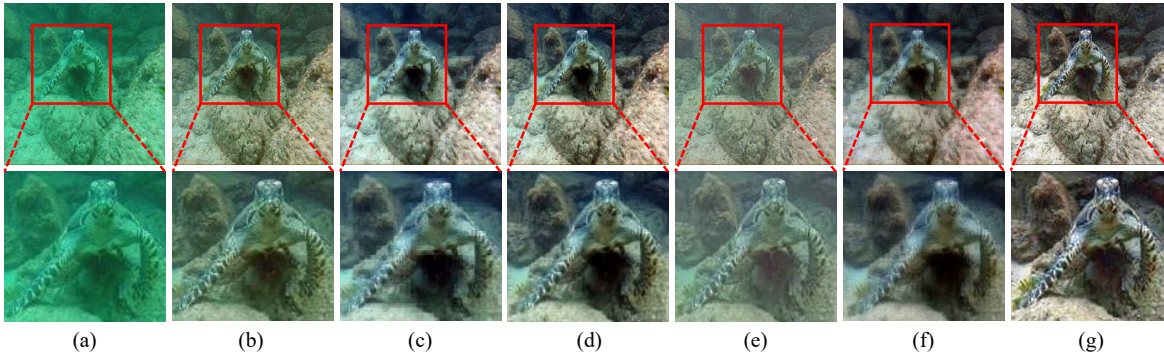


Fig. 13. Contribution of each component in the qualitative ablation study. From left to right, (a) Raw underwater image, (b) -w/o GCC: without global color correction, (c) -w/o CSDR: without cross-spectral detail refinement, (d) -w/o $\mathcal{L}_{details}$: without detail-preserving loss, (e) -w/o $\mathcal{L}_{content}$: without content loss, (f) -w/o HF-conditions: without refined high-frequency spectrum as input conditions, and (g) DiffColor: the full framework.

demonstrates the effectiveness of the loss functions $\mathcal{L}_{details}$ and $\mathcal{L}_{content}$, especially the latter is necessary to remove the foggy appearance of underwater images.

Effectiveness of GCC and CSDR Modules. In Table II, “-w/o GCC” means removing the global color correction module, while “-w/o CSDR” indicates that there is no cross-spectral detail refinement module to enrich image details. Compared with the whole DiffColor, their SSIM and PSNR scores are degraded on the Test-U100, Test-L500, and EUVP benchmarks, especially for the column of “-w/o GCC”. The decreased scores illustrate the necessity of color correction and detail refinement throughout the restoration process.

Loss Functions. In Table III, the “-w/o $\mathcal{L}_{details}$ ” denotes the removal of detail-preserving loss $\mathcal{L}_{details}$, which aims to ensure rich details of the restored image. Meanwhile “-w/o $\mathcal{L}_{content}$ ” indicates the removal of the content loss $\mathcal{L}_{content}$, leading to a noticeable decrease in both SSIM and PSNR metrics. This degradation is relatively significant compared to the removal of $\mathcal{L}_{details}$, which highlights the effectiveness of content-preserving loss in our training strategy.



Fig. 15. Enhanced results of low-light images from the *LOL* dataset [19]. The top are degraded low-light images from three scenes, while the bottom are enhanced results with our DiffColor method.



Fig. 16. Removal results of thin cloud images from the *MCGAN* dataset [88]. The top are four images with different cloud densities, while the bottom are cloud removal results with our DiffColor method.

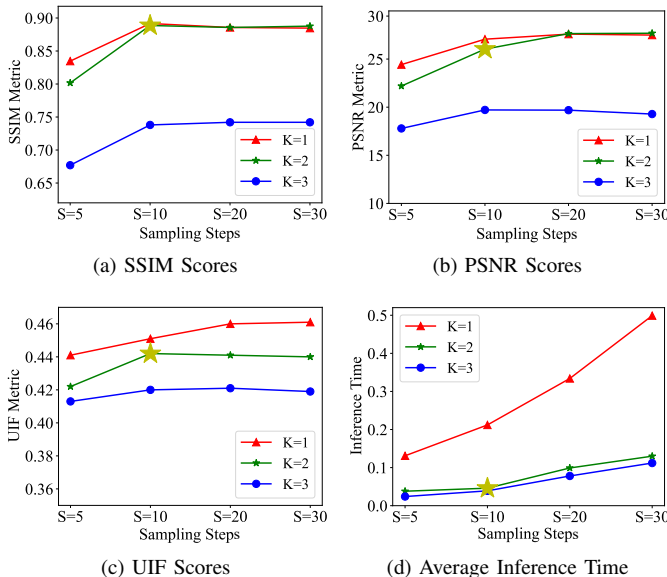


Fig. 14. Ablation studies of wavelet transform levels K and sampling steps S in terms of three full-reference metrics (SSIM, PSNR, UIF) and Inference Time. The results using the default settings are marked with a yellow asterisk.

High-frequency Spectrum as Conditional Input. In Table IV, “-w/o HF-Conditions” indicates that there is no refined high-frequency spectrum as input conditions for the diffusion model. Both SSIM and PSNR scores decrease compared to the full framework, demonstrating that using high-frequency signals as input conditions for the noise estimation network ensures high-fidelity content restoration even when starting from a randomly sampled noise in the reverse process.

Wavelet Transform Levels and Sampling Steps. We further provide an ablation study about wavelet transform levels K and sampling steps S . As shown in Fig. 14, we can observe that as the levels K of wavelet transform increases, the reduction of image spatial resolution brings inference acceleration, but the quality of enhancement decreases in terms of SSIM, PSNR and UIF metrics. Another trend is that the increase of sampling steps S leads to a clear increase in inference time, but beyond 20 sampling steps, most metrics exhibit minimal improvement. Considering the trade-off between inference time and the performance of image enhancement, we set $K = 2$ and $S = 10$ in the experiment.

F. Robustness and Generalization Validation

In this subsection, we also verify that the proposed DiffColor method can be directly generalized to other challenging image restoration tasks such as low-light image enhancement and thin cloud removal.

Compared with low-light images, underwater images exhibit more complex and variable degradation types, such as color distortion, foggy appearance, light vertigo, low contrast, etc., making the UIE task more challenging. Fig. 15 presents the qualitative comparison results of the low-light images selected from the LOL dataset [19]. The results indicate that our DiffColor effectively improves the low-light brightness of images while ensuring color integrity. In addition, we further conducted a robustness validation of DiffColor for thin cloud removal, with the results shown in Fig. 16. Removing thin clouds is more challenging compared to image dehazing due to its inhomogeneous distribution property. The experimental results show that our DiffColor effectively removes obscuring clouds from the images without exhibiting excessive enhancement in cloud-free regions.

V. CONCLUSION

This paper presents DiffColor, a color distribution-aware diffusion model for underwater image enhancement. DiffColor leverages the strong generative capability of diffusion models alongside the dimensionality reduction benefits of wavelet transformation, significantly reducing the computational resource consumption of traditional conditional diffusion models. Unlike single-noise image restoration tasks, DiffColor incorporates the GCC module to address global degradation commonly encountered in reverse denoising. For the sacrificed image details caused by underwater medium scattering, DiffColor employs the CSDR module to enhance high-frequency details and utilize refined high-frequency components as the conditional signal. Through qualitative and quantitative evaluations, we validate that DiffColor achieves state-of-the-art performance in underwater image restoration.

REFERENCES

- [1] Z. Zheng, H. Liang, B.-S. Hua, Y. H. Wong, P. Ang, A. P. Y. Chui, and S.-K. Yeung, "Coralscop: Segment any coral image on this planet," in *Proceedings of the IEEE/CVF Conference on Computer Vision and Pattern Recognition*, 2024, pp. 28 170–28 180.
- [2] P. Zhang, T. Yan, Y. Liu, and H. Lu, "Fantastic animals and where to find them: Segment any marine animal with dual sam," in *Proceedings of the IEEE/CVF Conference on Computer Vision and Pattern Recognition*, 2024, pp. 2578–2587.
- [3] Z. Liu, B. Wang, Y. Li, J. He, and Y. Li, "Unitmodule: A lightweight joint image enhancement module for underwater object detection," *Pattern Recognition*, vol. 151, p. 110435, 2024.
- [4] L. Cai, N. E. McGuire, R. Hanlon, T. A. Mooney, and Y. Girdhar, "Semi-supervised visual tracking of marine animals using autonomous underwater vehicles," *International Journal of Computer Vision*, vol. 131, no. 6, pp. 1406–1427, 2023.
- [5] Z. Wang, L. Shen, Y. Yu, and Y. Hui, "Uierl: Internal-external representation learning network for underwater image enhancement," *IEEE Transactions on Multimedia*, vol. 26, pp. 9252–9267, 2024.
- [6] N. Jiang, W. Chen, Y. Lin, T. Zhao, and C.-W. Lin, "Underwater image enhancement with lightweight cascaded network," *IEEE Transactions on Multimedia*, vol. 24, pp. 4301–4313, 2021.
- [7] P. Lin, Y. Wang, Y. Li, Z. Fan, and X. Fu, "Underwater color correction network with knowledge transfer," *IEEE Transactions on Multimedia*, vol. 26, pp. 8088–8103, 2024.
- [8] P. Guo, L. He, S. Liu, D. Zeng, and H. Liu, "Underwater image quality assessment: Subjective and objective methods," *IEEE Transactions on Multimedia*, vol. 24, pp. 1980–1989, 2022.
- [9] Y. Liu, B. Zhang, R. Hu, K. Gu, G. Zhai, and J. Dong, "Underwater image quality assessment: Benchmark database and objective method," *IEEE Transactions on Multimedia*, vol. 26, pp. 7734–7747, 2024.
- [10] K. Li, X. Wang, W. Liu, Q. Qi, G. Hou, Z. Zhang, and K. Sun, "Learning scribbles for dense depth: Weakly-supervised single underwater image depth estimation boosted by multi-task learning," *IEEE Transactions on Geoscience and Remote Sensing*, vol. 62, pp. 1–15, 2024.
- [11] K. Wu, J. Huang, Y. Ma, F. Fan, and J. Ma, "Cycle-retinex: Unpaired low-light image enhancement via retinex-inline cyclegan," *IEEE Transactions on Multimedia*, vol. 26, pp. 1213–1228, 2023.
- [12] G. Li, B. Zhao, and X. Li, "Low-light image enhancement with sam-based structure priors and guidance," *IEEE Transactions on Multimedia*, vol. 26, pp. 10854–10866, 2024.
- [13] L. Ma, R. Liu, Y. Wang, X. Fan, and Z. Luo, "Low-light image enhancement via self-reinforced retinex projection model," *IEEE Transactions on Multimedia*, vol. 25, pp. 3573–3586, 2023.
- [14] Q. Jiang, Y. Mao, R. Cong, W. Ren, C. Huang, and F. Shao, "Un-supervised decomposition and correction network for low-light image enhancement," *IEEE Transactions on Intelligent Transportation Systems*, vol. 23, no. 10, pp. 19440–19455, 2022.
- [15] P. W. Patil, S. Gupta, S. Rana, S. Venkatesh, and S. Murala, "Multi-weather image restoration via domain translation," in *Proceedings of the IEEE/CVF International Conference on Computer Vision*, 2023, pp. 21 696–21 705.
- [16] H. Sun, Z. Luo, D. Ren, B. Du, L. Chang, and J. Wan, "Unsupervised multi-branch network with high-frequency enhancement for image dehazing," *Pattern Recognition*, vol. 156, p. 110763, 2024.
- [17] C. Li, C. Guo, W. Ren, R. Cong, J. Hou, S. Kwong, and D. Tao, "An underwater image enhancement benchmark dataset and beyond," *IEEE Transactions on Image Processing*, vol. 29, pp. 4376–4389, 2020.
- [18] B. Li, W. Ren, D. Fu, D. Tao, D. Feng, W. Zeng, and Z. Wang, "Benchmarking single-image dehazing and beyond," *IEEE Transactions on Image Processing*, vol. 28, no. 1, pp. 492–505, 2018.
- [19] C. Wei, W. Wang, W. Yang, and J. Liu, "Deep retinex decomposition for low-light enhancement," *arXiv preprint arXiv:1808.04560*, 2018.
- [20] W. Zhang, P. Zhuang, H.-H. Sun, G. Li, S. Kwong, and C. Li, "Underwater image enhancement via minimal color loss and locally adaptive contrast enhancement," *IEEE Transactions on Image Processing*, vol. 31, pp. 3997–4010, 2022.
- [21] H. Wang, S. Sun, and P. Ren, "Underwater color disparities: Cues for enhancing underwater images toward natural color consistencies," *IEEE Transactions on Circuits and Systems for Video Technology*, pp. 1–1, 2023.
- [22] H. Song, L. Chang, Z. Chen, and P. Ren, "Enhancement-registration-homogenization (erh): A comprehensive underwater visual reconstruction paradigm," *IEEE Transactions on Pattern Analysis and Machine Intelligence*, vol. 44, no. 10, pp. 6953–6967, 2022.
- [23] L. Chang, H. Song, M. Li, and M. Xiang, "Uidef: A real-world underwater image dataset and a color-contrast complementary image enhancement framework," *ISPRS Journal of Photogrammetry and Remote Sensing*, vol. 196, pp. 415–428, 2023.
- [24] J. Zhou, S. Wang, Z. Lin, Q. Jiang, and F. Sohel, "A pixel distribution remapping and multi-prior retinex variational model for underwater image enhancement," *IEEE Transactions on Multimedia*, vol. 26, pp. 7838–7849, 2024.
- [25] G. Hou, N. Li, P. Zhuang, K. Li, H. Sun, and C. Li, "Non-uniform illumination underwater image restoration via illumination channel sparsity prior," *IEEE Transactions on Circuits and Systems for Video Technology*, vol. 34, no. 2, pp. 799–814, 2024.
- [26] Q. Jiang, Y. Zhang, F. Bao, X. Zhao, C. Zhang, and P. Liu, "Two-step domain adaptation for underwater image enhancement," *Pattern Recognition*, vol. 122, p. 108324, 2022.
- [27] J. Zhou, J. Sun, C. Li, Q. Jiang, M. Zhou, K.-M. Lam, W. Zhang, and X. Fu, "Hclr-net: Hybrid contrastive learning regularization with locally randomized perturbation for underwater image enhancement," *International Journal of Computer Vision*, pp. 1–25, 2024.
- [28] X. Xue, Z. Li, L. Ma, Q. Jia, R. Liu, and X. Fan, "Investigating intrinsic degradation factors by multi-branch aggregation for real-world underwater image enhancement," *Pattern recognition*, vol. 133, p. 109041, 2023.
- [29] S. Huang, K. Wang, H. Liu, J. Chen, and Y. Li, "Contrastive semi-supervised learning for underwater image restoration via reliable bank," in *Proceedings of the IEEE/CVF Conference on Computer Vision and Pattern Recognition*, 2023, pp. 18 145–18 155.

- [30] Q. Qi, Y. Zhang, F. Tian, Q. J. Wu, K. Li, X. Luan, and D. Song, "Underwater image co-enhancement with correlation feature matching and joint learning," *IEEE Transactions on Circuits and Systems for Video Technology*, vol. 32, no. 3, pp. 1133–1147, 2022.
- [31] Q. Qi, K. Li, H. Zheng, X. Gao, G. Hou, and K. Sun, "Sguie-net: Semantic attention guided underwater image enhancement with multi-scale perception," *IEEE Transactions on Image Processing*, vol. 31, pp. 6816–6830, 2022.
- [32] Q. Liu, Q. Zhang, W. Liu, W. Chen, X. Liu, and X. Wang, "Wds-gan: A weak-strong dual supervised learning method for underwater image enhancement," *Pattern Recognition*, vol. 143, p. 109774, 2023.
- [33] Y. Qing, Y. Wang, H. Yan, X. Xie, and Z. Wu, "Unformer: A transformer-based approach for adaptive multi-scale feature aggregation in underwater image enhancement," *IEEE Transactions on Artificial Intelligence*, pp. 1–14, 2024.
- [34] Y. Qing, S. Liu, H. Wang, and Y. Wang, "Diffuie: Learning latent global priors in diffusion models for underwater image enhancement," *IEEE Transactions on Multimedia*, pp. 1–14, 2024.
- [35] D. Du, E. Li, L. Si, W. Zhai, F. Xu, J. Niu, and F. Sun, "Uiedp: Boosting underwater image enhancement with diffusion prior," *Expert Systems with Applications*, vol. 259, p. 125271, 2025.
- [36] Q. Jiang, X. Yi, L. Ouyang, J. Zhou, and Z. Wang, "Towards dimension-enriched underwater image quality assessment," *IEEE Transactions on Circuits and Systems for Video Technology*, pp. 1–1, 2024.
- [37] Q. Jiang, Y. Kang, Z. Wang, W. Ren, and C. Li, "Perception-driven deep underwater image enhancement without paired supervision," *IEEE Transactions on Multimedia*, vol. 26, pp. 4884–4897, 2024.
- [38] Y. Liu, Q. Jiang, X. Wang, T. Luo, and J. Zhou, "Underwater image enhancement with cascaded contrastive learning," *IEEE Transactions on Multimedia*, pp. 1–14, 2024.
- [39] J. Song, C. Meng, and S. Ermon, "Denoising diffusion implicit models," *arXiv preprint arXiv:2010.02502*, 2020.
- [40] Y. Tang, H. Kawasaki, and T. Iwaguchi, "Underwater image enhancement by transformer-based diffusion model with non-uniform sampling for skip strategy," in *Proceedings of the 31st ACM International Conference on Multimedia*, 2023, pp. 5419–5427.
- [41] S. Lu, F. Guan, H. Zhang, and H. Lai, "Speed-up ddpm for real-time underwater image enhancement," *IEEE Transactions on Circuits and Systems for Video Technology*, vol. 34, no. 5, pp. 3576–3588, 2024.
- [42] C. Zhao, W. Cai, C. Dong, and C. Hu, "Wavelet-based fourier information interaction with frequency diffusion adjustment for underwater image restoration," in *Proceedings of the IEEE/CVF Conference on Computer Vision and Pattern Recognition*, 2024, pp. 8281–8291.
- [43] D. Akkaynak and T. Treibitz, "A revised underwater image formation model," in *Proceedings of the IEEE/CVF Conference on Computer Vision and Pattern Recognition*, 2018, pp. 6723–6732.
- [44] C. Li, S. Anwar, and F. Porikli, "Underwater scene prior inspired deep underwater image and video enhancement," *Pattern Recognition*, vol. 98, p. 107038, 2020.
- [45] J. Zhou, Q. Liu, Q. Jiang, W. Ren, K.-M. Lam, and W. Zhang, "Underwater camera: Improving visual perception via adaptive dark pixel prior and color correction," *International Journal of Computer Vision*, pp. 1–19, 2023.
- [46] P. Drews, E. Nascimento, F. Moraes, S. Botelho, and M. Campos, "Transmission estimation in underwater single images," in *Proceedings of the IEEE/CVF International Conference on Computer Vision Workshops*, 2013, pp. 825–830.
- [47] Y. T. Peng, K. Cao, and P. C. Cosman, "Generalization of the dark channel prior for single image restoration," *IEEE Transactions on Image Processing*, vol. 27, no. 6, pp. 2856–2868, 2018.
- [48] Z. Liang, X. Ding, Y. Wang, X. Yan, and X. Fu, "Gudcp: Generalization of underwater dark channel prior for underwater image restoration," *IEEE Transactions on Circuits and Systems for Video Technology*, vol. 32, no. 7, pp. 4879–4884, 2021.
- [49] C. O. Ancuti, C. Ancuti, C. De Vleeschouwer, and P. Bekaert, "Color balance and fusion for underwater image enhancement," *IEEE Transactions on Image Processing*, vol. 27, no. 1, pp. 379–393, 2018.
- [50] W. Zhang, Y. Wang, and C. Li, "Underwater image enhancement by attenuated color channel correction and detail preserved contrast enhancement," *IEEE Journal of Oceanic Engineering*, vol. 47, no. 3, pp. 718–735, 2022.
- [51] X. Fu, P. Zhuang, Y. Huang, Y. Liao, X.-P. Zhang, and X. Ding, "A retinex-based enhancing approach for single underwater image," in *2014 IEEE International Conference on Image Processing*, 2014, pp. 4572–4576.
- [52] P. Zhuang, J. Wu, F. Porikli, and C. Li, "Underwater image enhancement with hyper-laplacian reflectance priors," *IEEE Transactions on Image Processing*, vol. 31, pp. 5442–5455, 2022.
- [53] W. Zhang, L. Dong, and W. Xu, "Retinex-inspired color correction and detail preserved fusion for underwater image enhancement," *Computers and Electronics in Agriculture*, vol. 192, p. 106585, 2022.
- [54] D. Garg, N. K. Garg, and M. Kumar, "Underwater image enhancement using blending of clahe and percentile methodologies," *Multimedia Tools and Applications*, vol. 77, pp. 26 545–26 561, 2018.
- [55] D. Huang, Y. Wang, W. Song, J. Sequeira, and S. Mavromatis, "Shallow-water image enhancement using relative global histogram stretching based on adaptive parameter acquisition," in *2018 International Conference on MultiMedia Modeling*, 2018, pp. 453–465.
- [56] J. Zhou, L. Pang, D. Zhang, and W. Zhang, "Underwater image enhancement method via multi-interval subhistogram perspective equalization," *IEEE Journal of Oceanic Engineering*, vol. 48, no. 2, pp. 474–488, 2023.
- [57] C. Fabbri, M. J. Islam, and J. Sattar, "Enhancing underwater imagery using generative adversarial networks," in *2018 IEEE International Conference on Robotics and Automation*, 2018, pp. 7159–7165.
- [58] J. Li, K. A. Skinner, R. M. Eustice, and M. Johnson-Roberson, "Watergan: Unsupervised generative network to enable real-time color correction of monocular underwater images," *IEEE Robotics and Automation Letters*, vol. 3, no. 1, pp. 387–394, 2018.
- [59] M. J. Islam, Y. Xia, and J. Sattar, "Fast underwater image enhancement for improved visual perception," *IEEE Robotics and Automation Letters*, vol. 5, no. 2, pp. 3227–3234, 2020.
- [60] Y. Guo, H. Li, and P. Zhuang, "Underwater image enhancement using a multiscale dense generative adversarial network," *IEEE Journal of Oceanic Engineering*, vol. 45, no. 3, pp. 862–870, 2020.
- [61] R. Liu, Z. Jiang, S. Yang, and X. Fan, "Twin adversarial contrastive learning for underwater image enhancement and beyond," *IEEE Transactions on Image Processing*, vol. 31, pp. 4922–4936, 2022.
- [62] S. Sun, H. Wang, H. Zhang, M. Li, M. Xiang, C. Luo, and P. Ren, "Underwater image enhancement with reinforcement learning," *IEEE Journal of Oceanic Engineering*, pp. 1–13, 2022.
- [63] H. Wang, S. Sun, X. Bai, J. Wang, and P. Ren, "A reinforcement learning paradigm of configuring visual enhancement for object detection in underwater scenes," *IEEE Journal of Oceanic Engineering*, vol. 48, no. 2, pp. 443–461, 2023.
- [64] Y. Wang, J. Zhang, Y. Cao, and Z. Wang, "A deep cnn method for underwater image enhancement," in *2017 IEEE international conference on image processing (ICIP)*, 2017, pp. 1382–1386.
- [65] L. Chen, Z. Jiang, L. Tong, Z. Liu, A. Zhao, Q. Zhang, J. Dong, and H. Zhou, "Perceptual underwater image enhancement with deep learning and physical priors," *IEEE Transactions on Circuits and Systems for Video Technology*, vol. 31, no. 8, pp. 3078–3092, 2020.
- [66] H. Song, L. Chang, H. Wang, and P. Ren, "Dual-model: Revised imaging network and visual perception correction for underwater image enhancement," *Engineering Applications of Artificial Intelligence*, vol. 125, p. 106731, 2023.
- [67] Z. Wang, L. Shen, M. Xu, M. Yu, K. Wang, and Y. Lin, "Domain adaptation for underwater image enhancement," *IEEE Transactions on Image Processing*, vol. 32, pp. 1442–1457, 2023.
- [68] Y. Yin, D. Xu, C. Tan, P. Liu, Y. Zhao, and Y. Wei, "Cle diffusion: Controllable light enhancement diffusion model," in *Proceedings of the 31st ACM International Conference on Multimedia*, 2023, pp. 8145–8156.
- [69] X. P. Ooi and C. S. Chan, "Llde: Enhancing low-light images with diffusion model," in *2023 IEEE International Conference on Image Processing*, 2023, pp. 1305–1309.
- [70] S. Gao, X. Liu, B. Zeng, S. Xu, Y. Li, X. Luo, J. Liu, X. Zhen, and B. Zhang, "Implicit diffusion models for continuous super-resolution," in *Proceedings of the IEEE/CVF Conference on Computer Vision and Pattern Recognition*, 2023, pp. 10 021–10 030.
- [71] A. Lugmayr, M. Danelljan, A. Romero, F. Yu, R. Timofte, and L. Van Gool, "Repaint: Inpainting using denoising diffusion probabilistic models," in *Proceedings of the IEEE/CVF Conference on Computer Vision and Pattern Recognition*, 2022, pp. 11 461–11 471.
- [72] A. Wu, D. Chen, and C. Deng, "Deep feature deblurring diffusion for detecting out-of-distribution objects," in *Proceedings of the IEEE/CVF International Conference on Computer Vision*, 2023, pp. 13 381–13 391.
- [73] S. Lu, F. Guan, H. Zhang, and H. Lai, "Underwater image enhancement method based on denoising diffusion probabilistic model," *Journal of Visual Communication and Image Representation*, vol. 96, p. 103926, 2023.

- [74] D. Zhou, Z. Yang, and Y. Yang, "Pyramid diffusion models for low-light image enhancement," in *Proceedings of the Thirty-Second International Joint Conference on Artificial Intelligence*, 2023, pp. 1795–1803.
- [75] X. Jin, C. Lan, W. Zeng, Z. Chen, and L. Zhang, "Style normalization and restitution for generalizable person re-identification," in *proceedings of the IEEE/CVF conference on computer vision and pattern recognition*, 2020, pp. 3143–3152.
- [76] D. Berman, D. Levy, S. Avidan, and T. Treibitz, "Underwater single image color restoration using haze-lines and a new quantitative dataset," *IEEE transactions on pattern analysis and machine intelligence*, vol. 43, no. 8, pp. 2822–2837, 2021.
- [77] Z. Fu, W. Wang, Y. Huang, X. Ding, and K.-K. Ma, "Uncertainty inspired underwater image enhancement," in *European Conference on Computer Vision*, 2022, pp. 465–482.
- [78] K. Li, H. Fan, Q. Qi, C. Yan, K. Sun, and Q. J. Wu, "Tctl-net: Template-free color transfer learning for self-attention driven underwater image enhancement," *IEEE Transactions on Circuits and Systems for Video Technology*, vol. 34, no. 6, pp. 4682–4697, 2024.
- [79] L. Peng, C. Zhu, and L. Bian, "U-shape transformer for underwater image enhancement," *IEEE Transactions on Image Processing*, vol. 32, pp. 3066–3079, 2023.
- [80] W. Zhang, L. Zhou, P. Zhuang, G. Li, X. Pan, W. Zhao, and C. Li, "Underwater image enhancement via weighted wavelet visual perception fusion," *IEEE Transactions on Circuits and Systems for Video Technology*, vol. 34, no. 4, pp. 2469–2483, 2024.
- [81] D. Zhang, J. Zhou, C. Guo, W. Zhang, and C. Li, "Synergistic multiscale detail refinement via intrinsic supervision for underwater image enhancement," in *Proceedings of the AAAI Conference on Artificial Intelligence*, vol. 38, no. 7, 2024, pp. 7033–7041.
- [82] R. Hou, H. Chang, B. Ma, S. Shan, and X. Chen, "Cross attention network for few-shot classification," *Advances in Neural Information Processing Systems*, vol. 32, 2019.
- [83] R. Liu, X. Fan, M. Zhu, M. Hou, and Z. Luo, "Real-world underwater enhancement: Challenges, benchmarks, and solutions under natural light," *IEEE Transactions on Circuits and Systems for Video Technology*, vol. 30, no. 12, pp. 4861–4875, 2020.
- [84] C. Liu, Z. Wang, S. Wang, T. Tang, Y. Tao, C. Yang, H. Li, X. Liu, and X. Fan, "A new dataset, poisson gan and aquanet for underwater object grabbing," *IEEE Transactions on Circuits and Systems for Video Technology*, vol. 32, no. 5, pp. 2831–2844, 2021.
- [85] Y. Zheng, W. Chen, R. Lin, T. Zhao, and P. Le Callet, "Uif: An objective quality assessment for underwater image enhancement," *IEEE Transactions on Image Processing*, vol. 31, pp. 5456–5468, 2022.
- [86] M. Yang and A. Sowmya, "An underwater color image quality evaluation metric," *IEEE Transactions on Image Processing*, vol. 24, no. 12, pp. 6062–6071, 2015.
- [87] K. Panetta, C. Gao, and S. Agaian, "Human-visual-system-inspired underwater image quality measures," *IEEE Journal of Oceanic Engineering*, vol. 41, no. 3, pp. 541–551, 2016.
- [88] Z. Xu, K. Wu, L. Huang, Q. Wang, and P. Ren, "Cloudy image arithmetic: A cloudy scene synthesis paradigm with an application to deep-learning-based thin cloud removal," *IEEE Transactions on Geoscience and Remote Sensing*, vol. 60, pp. 1–16, 2021.